

## Linear, Collisionless, Bi-Maxwellian Neutral-Sheet Tearing Instability

G. R. Burkhart

*Science Applications International Corporation, 1710 Goodridge Drive, McLean, Virginia 22102*

James Chen

*Geophysical and Plasma Dynamics Branch, Plasma Physics Division, Naval Research Laboratory, Washington, D.C. 20375*

(Received 6 March 1989)

The long-standing problem of the linear, bi-Maxwellian neutral-sheet tearing instability is solved without recourse to an approximation of the orbits or the constant- $\psi$  approximation. We are therefore able to consider regimes beyond the validity of previous theories. As the temperature anisotropy is increased, the growth rate increases and the wavelength associated with the peak growth decreases.

PACS numbers: 52.35.Py

The collisionless tearing instability has been studied both in the laboratory<sup>1,2</sup> and in the geophysical context as a possible explanation for the onset of reconnection.<sup>3</sup> In the neutral-sheet geometry, the magnetic field reverses direction and particles near the magnetic null execute complicated trajectories. Although the collisionless tearing instability of Maxwellian and bi-Maxwellian neutral sheets has been studied for over twenty years,<sup>4-15</sup> no solution of the linear problem has been given which does not use approximate orbits or an assumed form for the eigenfunction (e.g., the constant- $\psi$  approximation). Recently, the instability in neutral sheets with temperature anisotropy<sup>9,10</sup> has attracted renewed interest.<sup>11,12,14,16</sup> The linear growth rate of the isotropic tearing instability is generally too small to explain the observed time scale for the onset of geomagnetic substorms. One possible resolution of the problem is the inclusion of an ion temperature anisotropy,<sup>17</sup> which enhances the growth rate considerably. However, it was found that differing levels of sophistication in treating the unmagnetized ion orbits can lead to widely differing growth rates,<sup>11</sup> indicating that an exact treatment of the orbits is critical. In this Letter we will present the results of the first study of the linear collisionless tearing instability in a bi-Maxwellian neutral sheet which employs neither approximate orbits nor an assumed form for the eigenfunction of the perturbations.

For this work, the equilibrium is taken to be the Harris equilibrium,<sup>18</sup>  $\mathbf{B} = B_0 \tanh(z/\delta) \hat{\mathbf{e}}_x$ , that includes a bi-Maxwellian velocity distribution,  $f_0[(H_\perp - VP_y)/T_\perp, H_\parallel/T_\parallel]$ . In the classic studies the perturbations of the fields are represented by  $A_y^1(x, z, t) = \psi(z) \times \exp(ikx + \gamma t)$ , where  $A_y^1$  is the  $y$  component of the perturbed vector potential. The electrostatic potential is not necessary provided  $\rho_0/\delta$  is small compared to unity in the isotropic case.<sup>13</sup> In the anisotropic case, the effect of the electrostatic potential has yet to be evaluated.

The growth rate and eigenfunctions are obtained from Ampère's law,

$$-\frac{\partial^2 \psi}{\partial z^2} + k^2 \psi = \frac{4\pi}{c} J_y^1, \quad (1)$$

where the perturbed current is given by

$$J_y^1 = \sum q \int d^3 v v_y \left[ \frac{\partial f^0}{\partial P_y} \frac{\partial P_y}{\partial A_y} \psi + \frac{\partial f_0}{\partial H_\perp} \delta H_\perp + \frac{\partial f_0}{\partial H_\parallel} \delta H_\parallel \right]. \quad (2)$$

The perturbed distribution function is determined by the single-particle response to the perturbed fields,

$$\delta H_\perp = \frac{q}{c} \int_{-\infty}^t dt' v_y [cE_y^1 - v_x B_z^1], \quad (3)$$

$$\delta H_\parallel = \frac{q}{c} \int_{-\infty}^t dt' v_x v_y B_z^1. \quad (4)$$

Performing the integrations of Eqs. (3) and (4) is difficult and has been traditionally accomplished by using various approximations both on  $\psi$  and on the unperturbed orbits. In most analyses physical space is divided into two regions, an outer region, with  $|z| > d_e$ , and an inner region, having  $|z| < d_e$ . The parameter  $d_e$  is usually chosen to be  $d_e = (2\rho_e \delta)^{1/2}$ . In the outer region the electron orbits are assumed to be fully magnetized, while in the inner region the trajectories are approximated by those of free particles colliding elastically with barriers at  $z = \pm d_e$ . The inner-region current required to match the inner-region and outer-region eigenfunctions is produced by the acceleration of the unmagnetized inner-region charges by the induction electric field. By demanding the matching condition that  $d(\ln\psi)/dz$  be continuous at  $z = \pm d_e$ , the magnitude of the induction electric field and hence the growth rate of the perturbation are determined.

Chen and Palmadesso<sup>11</sup> found that a moderate ion temperature anisotropy of  $T_{i\perp}/T_{i\parallel} \approx 1.2-1.5$  increased the growth rate by 1 to 2 orders of magnitude. This was later confirmed by simulation results.<sup>12</sup> Another major result of Ref. 11 was the identification of an ion-intermediate region within which the ion orbits were taken to be of the unmagnetized type but the electron orbits were taken to be magnetized (the "three-region" approximation). It was found that the inclusion of this region in the calculation increased the growth rate by nearly an order of magnitude over calculations using only the two

regions for the anisotropic case. The conclusion of Ref. 9 that the ions are unimportant, which is based upon the two-region approximation, was thus found to be incorrect in the ion anisotropic case. This realization led Chen and Lee<sup>19,20</sup> to develop a method in which growth rates could be calculated taking into account all of the orbits exactly and without assuming the form of  $\psi$ . This is possible in the neutral-sheet geometry because all of the orbits are periodic in  $z$ . The integrals in Eqs. (3) and (4) may then be expanded in a sum of integrals over the orbit,

$$\int_{-\infty}^t dt' v_y(z') \psi(z') e^{(ikv_x + \gamma)(t' - t)} \\ = \sum_n \frac{1}{\gamma + ikv_x + in\Omega} \int_0^T dt' v_y(z') \psi(z') e^{-in\Omega t'}$$

where  $\Omega$  is the frequency and  $T$  the period of this orbit. The low-frequency approximation may now be invoked, leaving only the  $n=0$  response. The eigenfunction,  $\psi$ , is then expanded in a set of linearly independent basis functions (in this case, chapeau basis functions). Ampère's law, Eq. (1), can be represented as a matrix equation and the eigenvalues calculated numerically. The growth rate is then varied until an eigenvalue becomes zero. In Ref. 19 this method was applied to the case of a  $\delta$ -function distribution in  $H_{\perp}$ . However, this is not directly applicable to the magnetosphere since neither the isotropic Maxwellian nor the bi-Maxwellian is a possible limit of the  $\delta$ -function distribution.

In the present work, we have applied this method to the neutral sheet with a bi-Maxwellian distribution function and, for the first time, obtained solutions of Eq. (1) without using approximate orbits, or assuming the form for  $\psi$ . Details of the application and a comparison to the approximate theory of Chen and Palmadesso will be presented elsewhere.<sup>21</sup>

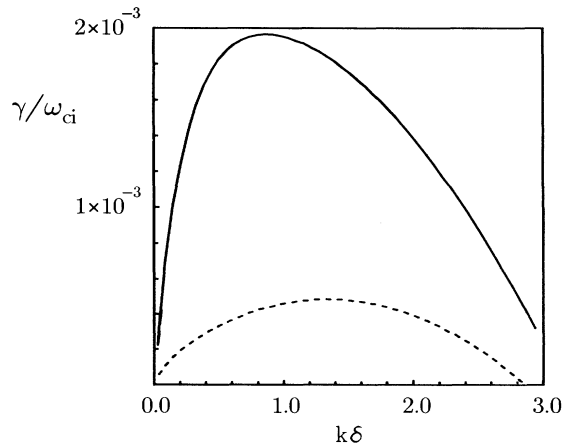


FIG. 1. The growth rate as a function of wave number for  $\rho_i/\delta=1/10$  and  $T_{i\perp}/T_{i\parallel}=1.2$ . The solid curve is the result if no approximations are made on the eigenfunction and the orbits; the dashed curve is the three-region result.

In Fig. 1, we show the dispersion relation for the case of  $\rho_i/\delta=1/10$  and  $T_{i\perp}/T_{i\parallel}=1.2$ . The solid curve is obtained by solving Eq. (1) with no approximation for the orbits or for  $\psi$ . The dashed line is the result of the three-region approximation.<sup>11</sup> For all of our results, we have used an isotropic electron distribution with  $T_e/T_{i\perp}=0.1$ , which is typically used in studies of the magnetotail. We should note that our boundary conditions are that  $\psi(z) \rightarrow \exp(-k|z|)$  as  $|z| \rightarrow \infty$ . A second possibility, fixing  $\psi'(H)/\psi(H)$ , can lead to enhanced growth<sup>15</sup> for  $kH \lesssim 1$ . The peak growth rate of the solid curve,  $\gamma_{\max}/\omega_{ci}$  at  $k\delta=0.8$ , is approximately 5 times greater than the corresponding result of the three-region treatment, the best previous approximation.

In Fig. 2, we show the dependence of the peak growth rate  $\gamma_{\max}$  on the ion temperature anisotropy for five values of  $\rho_i/\delta$  between  $\rho_i/\delta=1/100$  and  $\rho_i/\delta=1/2$ . Curves a-e correspond, respectively, to  $\rho_i/\delta=1/100, 1/20, 1/10, 1/4,$  and  $1/2$ . In each case, we see an enhancement in the growth rate by the ion anisotropy. In addition, the degree of the enhancement is greater for smaller values of  $\rho_i/\delta$ .

A qualitative understanding of the growth-rate enhancement can be found by considering the orbit integrals in Eqs. (3) and (4) and then using  $\delta H_{\perp}$  and  $\delta H_{\parallel}$  in the equation for the perturbed current, Eq. (2). We will use approximate orbits for our qualitative discussion even though the treatment employed in this work uses the exact orbits. In general, the adiabatic current [the first term in Eq. (2)] dominates the contributions of  $\delta H_{\perp}$  and  $\delta H_{\parallel}$  for the magnetized orbits far from the null plane. But on the other hand, the contribution due to

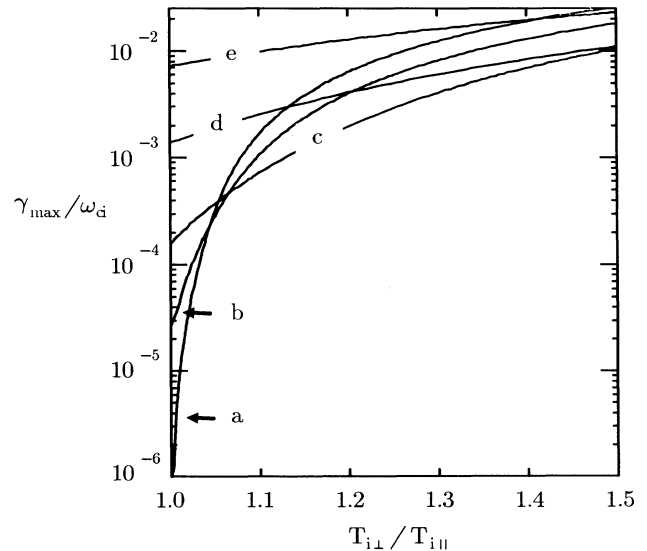


FIG. 2. The peak growth rate as a function of ion temperature anisotropy. For curve a,  $\rho_i/\delta=1/100$ ; for b,  $\rho_i/\delta=1/20$ ; for c,  $\rho_i/\delta=1/10$ ; for d,  $\rho_i/\delta=1/4$ ; for e,  $\rho_i/\delta=1/2$ .  $T_{e\perp}=T_{e\parallel}=0.1T_{i\perp}$  for all of our results.

straight-line orbits near the null plane is commensurate with, or dominates, the adiabatic current. Generally, the perturbed fields perturb the current through the unmagnetized particles in two ways. The first way is through the acceleration of the charges by the induction electric field  $E_y^1$ , represented by the first term in Eq. (3), and the second is through the rotation of the velocity vectors by  $B_z^1$ . In the isotropic case, the terms involving  $B_z^1$  in  $\delta H_\perp$  and  $\delta H_\parallel$  cancel when included in the perturbed current and integrated over the velocity distribution, leaving only the contribution from the term containing  $E_y^1$ . In the anisotropic case the terms containing  $B_z^1$  do not cancel, and instead yield a second contribution to the perturbed current. For a temperature anisotropy  $\alpha > 0$  [where  $\alpha = (T_\perp/T_\parallel - 1)$ ] in either the ion or electron distribution, it can be shown that this contribution to the current partially cancels the current due to the induction electric field. For  $\alpha < 0$  the effect is the opposite. Since the adiabatic current is the dominant contribution in the magnetized region, the relationship between the external perturbed field and the perturbed field near the null plane, which for the two-region or three-region approximation is expressed in the form of matching conditions, must be roughly the same in the anisotropic case as in the isotropic case. Physically, the net perturbed current near the null plane (the sum of the contributions due to  $E_y^1$  and  $B_z^1$ ) is determined by the overall geometry of the perturbation, essentially irrespective of the degree of anisotropy in the unmagnetized orbits. Thus, in the anisotropic case, the induction electric field must drive a greater current to make up for the canceling effect of  $B_z^1$  which means that the growth rate of the perturbation must be larger than in the isotropic case.

In Fig. 3, we show the dependence of the characteristic wavelength (the wavelength of the fastest growing mode,  $\lambda_x = 2\pi/k_{max}$ ) on  $\rho_i/\delta$  for five different values of the temperature anisotropy. Curves *a* through *e* corre-

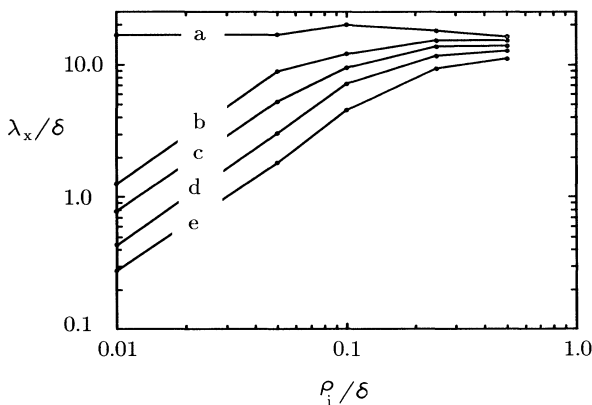


FIG. 3. The wavelength at the peak in the growth rate as a function of  $\rho_i/\delta$ . For curve *a*,  $T_{i\perp}/T_{i\parallel} = 1.0$ ; for *b*,  $T_{i\perp}/T_{i\parallel} = 1.05$ ; for *c*,  $T_{i\perp}/T_{i\parallel} = 1.1$ ; for *d*,  $T_{i\perp}/T_{i\parallel} = 1.2$ ; for *e*,  $T_{i\perp}/T_{i\parallel} = 1.5$ .

spond to temperature anisotropies 1.0, 1.05, 1.1, 1.2, and 1.5, respectively. In the isotropic case, curve *a*, the peak wavelength is about  $15\delta$ , and essentially independent of  $\rho_i/\delta$ . For sufficiently large values of the anisotropy,  $\alpha_i > \rho_i/\delta$  the characteristic wavelength becomes proportional to the ion gyroradius for a constant magnetic scale length. For  $\rho_i/\delta \lesssim 0.05$  and  $T_{i\perp}/T_{i\parallel} \gtrsim 1.5$ , the characteristic wavelength becomes comparable to the magnetic scale length or smaller. Considering the peak growth rate as a function of  $\rho_i/\delta$  for these same values of the temperature anisotropy, Fig. 4 also shows a change in behavior between the nearly isotropic tearing instability and the anisotropic instability with  $\alpha_i \gtrsim \rho_i/\delta$ . For the isotropic case, curve *a*, the growth rate adopts the expected dependence upon  $(\rho_i/\delta)^{5/2}$ . For larger temperature anisotropies,  $\alpha_i \gtrsim \rho_i/\delta$ , the growth rate *increases* with *decreasing* values of  $\rho_i/\delta$ .

The striking change in the characteristics of the instability as the ion temperature is increased above  $\alpha_i \gtrsim \rho_i/\delta$  leads one to classify the anisotropic instability as a different instability from the isotropic tearing instability. Clearly, for the anisotropic instability the free energy is dominated by the nonthermal distribution rather than the magnetic field gradient. Indeed, case *e* of Fig. 4 (for  $\rho_i/\delta \lesssim 0.1$ ) may be interpreted as a reduction in the growth rate of the anisotropic instability by the increasing magnetic field gradient (since we can view an increase in the parameter  $\rho_i/\delta$  as a decrease in  $\delta$  with  $\rho_i$  fixed). The growth rate only increases with an increasing magnetic field gradient when  $\alpha_i \lesssim \rho_i/\delta$  (for example,  $\rho_i/\delta \sim 0.25$  for case *e*). In the collisional case, this change in behavior led Shi, Lee, and Fu<sup>16</sup> to classify the instability for large temperature anisotropy as a mirror instability rather than a tearing instability.

Characteristic values of the parameter  $\rho_i/\delta$  in the Earth's magnetotail, for example, can vary widely depending upon the distance from the Earth and conditions in the solar wind. For 1-keV protons in a  $2 \times 10^{-4}$ -G field, a magnetic scale length of one Earth radius gives

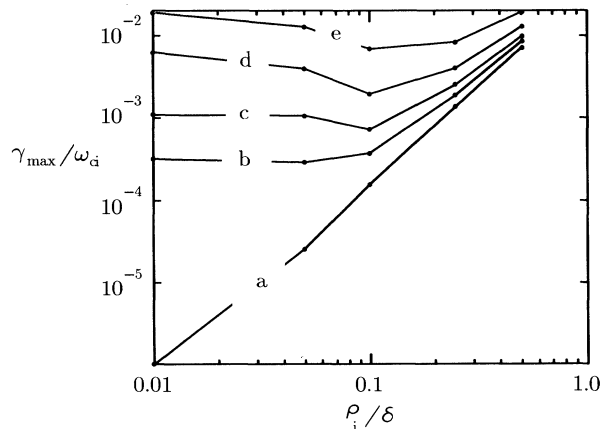


FIG. 4. The peak growth rates for the cases of Fig. 3.

$\rho_i/\delta=1/40$ . Values of  $\rho_i/\delta$  for the Earth's magnetotail may be larger than this estimate under different conditions. Field-reversed-configuration fusion experiments usually operate in the regime of  $\rho_i/\delta \approx 1/10$ , although fusion energy requirements may force a decrease in this parameter.<sup>22</sup> In both of these situations, then, a small temperature anisotropy could greatly affect the time scale for the onset of reconnection. In some scenarios, compression of the current sheet continues until the tearing-mode growth time is small compared to the time scale of the compression. The existence or the development of an ion temperature anisotropy could significantly increase the current sheet width finally reached before the onset of the instability.

We have found<sup>21</sup> that in the isotropic case, the three-region approximation underestimates the growth rate by more than an order of magnitude for  $\rho_i/\delta \lesssim 0.05$ . For the anisotropic case, an order-of-magnitude error also results for anisotropies  $\alpha_i \gtrsim \rho_i/\delta$ . For the limited range of  $0.05 \lesssim \rho_i/\delta \lesssim 0.5$  and  $\alpha_i \lesssim \rho_i/\delta$  the error is less than a factor of 2. Thus, consideration of the stability of the magnetotail or of a field-reversed configuration which has even a moderate anisotropy  $T_{\perp}/T_{\parallel} \gtrsim 1.1$  requires the use of this full solution.

In conclusion, we have solved the collisionless tearing-mode problem in a neutral sheet with Maxwellian and bi-Maxwellian distributions. Since our solution does not use approximations on the equilibrium orbits or the eigenfunction  $\psi$ , the range of validity is greatly expanded over the best previous approximation, the three-region approximation. The results show that with increasing  $T_{i\perp}/T_{i\parallel}$ , the linear growth rate increases (Figs. 2 and 4). For  $\alpha_i \gtrsim \rho_i/\delta$  the instability exhibits a behavior which is qualitatively different than the usual isotropic tearing mode (Figs. 3 and 4). Note that increased  $T_{i\perp}/T_{i\parallel}$  decreases the characteristic wavelength ( $\lambda_x$  in Fig. 3). We suggest that if small-island formation ( $\lambda_x < 10\delta$ ) is observed in experiments then temperature anisotropy may be present. On the other hand, a phase of island coalescence<sup>23</sup> is thought to follow the linear growth phase<sup>12,14,17</sup> so that the final island size could be larger than that predicted on the basis of linear theory.

Useful discussions with Y. C. Lee and J. F. Drake are appreciated. This research has been supported by U.S. Office of Naval Research and by NASA.

<sup>1</sup>R. L. Stenzel and W. Gekelman, Phys. Rev. Lett. **42**, 1055 (1979).

<sup>2</sup>J. H. Irby, J. F. Drake, and H. R. Griem, Phys. Rev. Lett. **42**, 228 (1979).

<sup>3</sup>A. Nishida, in *Magnetic Reconnection in Space and Laboratory Plasmas*, edited by E. W. Hones, Jr., Geophysical Monograph Series Vol. 30 (American Geophysical Union, Washington, D.C., 1984), p. 159.

<sup>4</sup>H. P. Furth, Nucl. Fusion Suppl., Pt. **1**, 169 (1962).

<sup>5</sup>D. Pfirsch, Z. Naturforsch. **17a**, 861 (1962).

<sup>6</sup>G. Laval and R. Pellat, C. R. Acad. Sci. **259**, 1706 (1964).

<sup>7</sup>G. Laval, R. Pellat, and M. Vuillemin, in *Plasma Physics and Controlled Nuclear Fusion Research* (International Atomic Energy Agency, Vienna, 1966), Vol. 2, p. 259.

<sup>8</sup>B. Coppi, G. Laval, and R. Pellat, Phys. Rev. Lett. **16**, 1207 (1966).

<sup>9</sup>D. W. Forslund, Ph.D. thesis, Princeton University, 1968 (unpublished).

<sup>10</sup>G. Laval and R. Pellat, in *Proceedings of the ESRIN Study Group, Frascati, Italy* (European Space Research Organization, Neuilly-sur-Seine, France, 1968), p. 5.

<sup>11</sup>J. Chen and P. Palmadesso, Phys. Fluids **27**, 1198 (1984).

<sup>12</sup>John Ambrosiano, Lou C. Lee, and Z. F. Fu, J. Geophys. Res. **91**, 113 (1986).

<sup>13</sup>M. Hoshino, J. Geophys. Res. **92**, 7368 (1987).

<sup>14</sup>D. W. Hewett, G. E. Frances, and C. E. Max, Phys. Rev. Lett. **61**, 893 (1988).

<sup>15</sup>W. Horton and T. Tajima, J. Geophys. Res. **93**, 2741 (1988).

<sup>16</sup>Y. Shi, L. C. Lee, and Z. F. Fu, J. Geophys. Res. **92**, 12171 (1987).

<sup>17</sup>J. Chen and P. J. Palmadesso, in *Magnetotail Physics*, edited by A. T. Y. Lui (Johns Hopkins Univ. Press, Baltimore, MD, 1987), p. 321.

<sup>18</sup>E. G. Harris, Nuovo Cimento **23**, 115 (1962).

<sup>19</sup>J. Chen and Y. C. Lee, Phys. Fluids **28**, 2137 (1985).

<sup>20</sup>J. Chen and Y. C. Lee, Phys. Fluids **11**, 2944 (1988).

<sup>21</sup>G. R. Burkhart and J. Chen (to be published).

<sup>22</sup>E. Sevillano and F. L. Ribe, in Ref. 3, p. 313.

<sup>23</sup>J. M. Finn and P. K. Kaw, Phys. Fluids **20**, 72 (1977).